Available online at www.sciencedirect.com
ScienceDirect
Ceramics International 36 (2010) 2163–2167
CERAMICS INTERNATIONAL
www.elsevier.com/locate/ceramint

Proton conductive YSZ-phosphate composite electrolyte for H_2S SOFC

Heng Chen, Zhengrong Xu, Cheng Peng [1], Zhicong Shi [2], Jing-Li Luo *, Alan Sanger, Karl T. Chuang

Department of Chemical and Materials Engineering, University of Alberta, Edmonton, AB, Canada T6G 2G6

Received 6 October 2009; received in revised form 12 April 2010; accepted 6 May 2010
Available online 25 June 2010

Abstract

A new oxide-salt composite electrolyte, YSZ–K_3PO_4–$Ca_3(PO_4)_2$, shows proton conductivity in the order of 10^{-2} S/cm at 700 °C. The proton transport number, determined using a hydrogen concentration cell, rises from more than 93% at 550 °C to 99% at 700 °C. The composite electrolyte is chemically stable in H_2S containing atmosphere, and so is a good candidate electrolyte material for H_2S solid oxide fuel cells applications.
© 2010 Elsevier Ltd and Techna Group S.r.l. All rights reserved.

Keywords: YSZ-phosphate composite Electrolyte; Proton conductivity; H_2S; SOFC

1. Introduction

H_2S is a corrosive and poisonous gas which is generated largely as a by-product of the refining of fossil fuels. The Claus process is used to oxidize H_2S to element sulfur. However, the overall energy efficiency of this process is unsatisfactory, as the chemical energy of the reaction is either vented or recovered only as low grade heat. In 1987, Pujare et al. first reported a direct H_2S-air solid oxide fuel cell (SOFC) to process H_2S [1]. Other researchers now have investigated H_2S as a fuel gas for a fuel cell because of its potential economical and environmental benefits [2–4]. At present, most fuel cells use yttria stabilized zirconia (YSZ) as electrolyte due to its sufficient oxygen ionic conductivity [5,6]. However, the products of the anode reaction in H_2S SOFCs based on YSZ electrolyte are water and sulfur dioxide (or mixtures with S_x), which have to be separated later so that the acid pollutant is not emitted. In contrast, H_2S fuel cells using a proton-conductor electrolyte do not have this problem. The only product at the anode side is sulfur, which can be condensed as a useful and environmentally benign product, and the product at the cathode side is clean water. Hence a significant focus of recent research is to find a stable electrolyte material with high proton conductivity for H_2S SOFCs.

BCY, $Ba(Ce_{1-x}Y_x)O_{3-\delta}$, is a typical proton conductor [7]. However, it is not stable in H_2S atmosphere. Li_2SO_4 and its composites are proton conductors and stable in H_2S [8]. However, Li_2SO is reduced to Li_2S and LiOH in H_2 atmosphere. Further, H_2S decomposes to an equilibrium mixture with hydrogen and sulfur at high temperatures ($T \geq 600$ °C) (Eq. (1)).

$$xH_2S \leftrightarrow xH_2 + S_x \quad (1)$$

The equilibrium concentration of H_2 increases quickly as the temperature rises. Consequently, Li_2SO_4 electrolyte is not stable during long-term operation of high temperature H_2S fuel cells, due to the decomposition of H_2S at operation temperatures above 600 °C. Recent research showed that ion-conducting ceramic composites with high chemical and thermal stability and low fabrication cost have high potential for use as electrolyte membranes. Zhu reported ceramic composites that had high ion conductivity and wide application in fuel cells [9]. Wei et al. determined the properties of Li_2SO_4–Al_2O_3 membrane as a H_2S fuel cell electrolyte [10]. Liu et al. reported a novel way of using doped CeO_2–$Ca_3(PO_4)_2$–K_3PO_4 composite, which is proton conductive, to synthesize ammonia from natural gas [4]. In the previous studies, the composites comprising an oxygen ion conductor and one or more phosphate salts showed high proton conductivities. The

* Corresponding author. Tel.: +1 780 492 2232; fax: +1 780 492 2881.
E-mail address: jingli.luo@ualberta.ca (J.-L. Luo).
[1] Permanent address: School of Chemistry and Chemical Engineering, South China University of Technology, Guangzhou, 510641, China.
[2] Current address: College of Chemical Engineering, Dalian University of Technology, #132, 158-Zhongshan Street, Dalian 116012, China.

0272-8842/$36.00 © 2010 Elsevier Ltd and Techna Group S.r.l. All rights reserved.
doi:10.1016/j.ceramint.2010.06.002

detailed mechanism of proton conduction in this kind of ceramic-salt composite material is still not clear yet, however, the material itself is very promising for potential applications.

Now we have developed new proton conducting YSZ-phosphate composite materials for potential application as electrolyte in H_2S SOFC. Hydrogen concentration cell techniques were used to measure the proton conductivity and transfer number. Other techniques, such as XRD and XPS were applied to determine the stability of the material in various environments.

2. Experimental

2.1. Materials preparation

The binary phosphate, K_3PO_4–$Ca_3(PO_4)_2$, with weight ratio 60 wt% $Ca_3(PO_4)_2$: 40 wt% K_3PO_4 was synthesized from potassium phosphate (K_3PO_4, Fisher), calcium hydroxide ($Ca(OH)_2$, Fisher), and phosphoric acid (H_3PO_4, Aldrich) [11]. Mixtures comprising different proportions of 8% yttria-stabilized zirconia powder (YSZ, Inframat Advanced Materials) and the combined binary phosphates were ball milled for 24 h. The proportions of binary phosphate in the composites were 9%, 12%, 15%, 18% and 27%. After drying, the composite powders was pressed into round pellets and the green bodies, enveloped in the same powders, were placed in a covered alumina crucible and sintered at 1400 °C for 10 h. For comparison, an alumina–phosphate composite also was prepared using the same procedure. The sintered disks were polished to ca. 1 mm thickness for conductivity tests and for determination of transport numbers using a hydrogen concentration cell.

2.2. Stability

The cross-sectional microstructures were determined using scanning electron microscopy (SEM, JEOL JAMP-9500F). To investigate the chemical stability of the composites, samples of the composites were heated in H_2 or H_2S atmosphere at 750 °C for 90 h in a quartz tube. Then X-ray diffraction (XRD, Rigaku Rotaflex X-ray diffractometer, 10–120° 2θ) and X-Ray Photoelectron Spectroscopy (XPS, Perkin-Elmer Corporation) analyses were used to compare compositions of the fresh and heated samples.

2.3. Cell preparation and electrochemical characterization

Platinum paste (Pt, Heraeus CL11-5100) was applied and then dried to form electrode catalyst at both sides of composite electrolyte membranes. The membrane electrode assembly (MEA) was sintered at 950 °C for 2 h. Before electrochemical testing, the MEA was heated at 600 °C for 4 h in hydrogen. The conductivity of samples was measured in hydrogen in the temperature range 550–750 °C by AC impedance method using a Solartron electrochemical measurement system (SI 1287 + SI 1260).

Hydrogen concentration cell tests were performed in a tubular furnace (Thermolyne F79300). Glass sealant (AREMCO-SEAL 617) was used to seal the alumina tubes to prevent gas leakage. Pure hydrogen (Praxair, PP4.5) and 1.05% hydrogen balanced with argon (Praxair) were used as anode and cathode gases respectively in the hydrogen concentration cell. The gas flow rates at both sides were 10 mL/min.

3. Results and discussion

3.1. Stability

Fig. 1 shows the XRD pattern of both fresh (after sintering) and treated samples of YSZ–K_3PO_4–$Ca_3(PO_4)_2$ composite in which the weight ratio of binary phosphates was 12% (abbreviated as YKC-12, hereafter) and, for comparison, the XRD pattern of YSZ. The XRD pattern of fresh composite after 1400 °C sintering (Fig. 1b) is essentially the same as that of pure YSZ (Fig. 1a). No peak was detected for any crystalline salt phase in the composite, and so the phosphates probably were present as an amorphous phase between the YSZ grains. The absence of any new peaks in the spectrum of fresh YKC-12 also showed that there was no chemical reaction of the phosphates with YSZ to form a new crystalline phase. Fig. 1c and d show the XRD patterns of YKC-12 composite after heating in H_2 and H_2S, respectively. There was no significant difference between either of these two treated samples (Fig. 1c and d) and the fresh sample (Fig. 1b), showing that neither H_2 nor H_2S had any effect on the YSZ phase structure.

The SEM image of the cross-section surface of YKC-12 (Fig. 2) showed that YSZ–K_3PO_4–$Ca_3(PO_4)_2$ composite membrane was dense, with particle size about 1–4 μm. The interconnection of the material indicates that salts are located at the boundaries among YSZ grains, resulting from melting and spreading of phosphates on the surface of YSZ particles during sintering, then solidification as the process temperature subsequently was reduced.

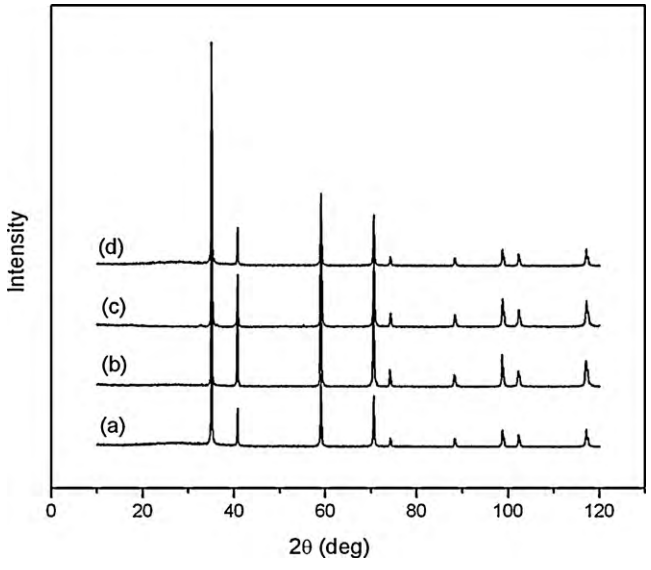

Fig. 1. XRD spectra of fresh YSZ (a), YKC-12 composite (b), and YKC-12 composite after heating in H_2 (c) and H_2S (d).

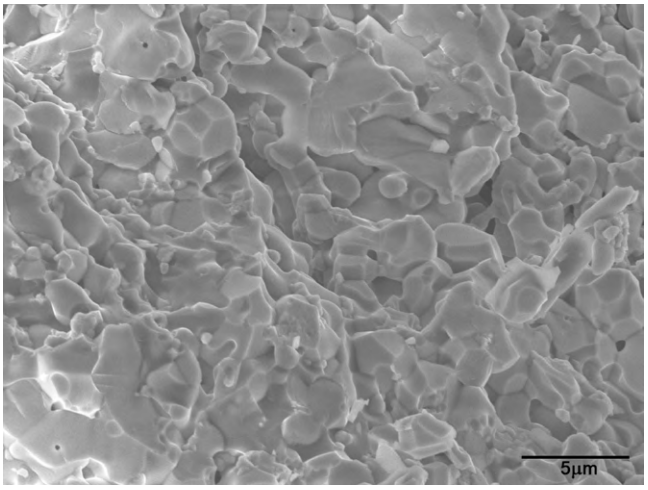

Fig. 2. SEM of the cross-section surface of the YKC-12 composite.

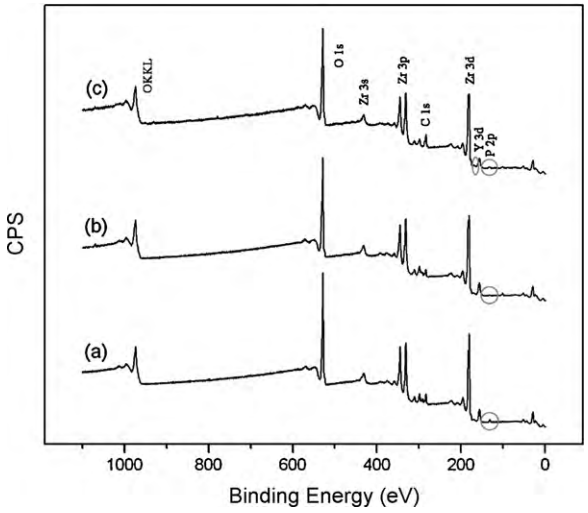

Fig. 3. XPS of YKC-12 composites before (a) and after heating in H_2 (b) or H_2S (c) at 750 °C for 90 h.

XPS analysis was performed to determine the chemical stability of the composite, and results are shown in Fig. 3. All spectra were calibrated to the C 1s emission (285 eV) arising from surface contamination. Spectra 3a, 3b and 3c respectively show XPS of fresh YKC-12 composite, and treated samples after H_2 and H_2S stability tests. There were no differences among these three XPS patterns. For more refined comparison, high resolution XPS was performed in the vicinity of element P 2p (128–140 eV) and S 2p (160–172 eV), shown in Fig. 4, which areas are identified by circle and ellipses in Fig. 3. The peak for P 2p in the spectrum of fresh YKC-12 composite was located approximately in 133.2 eV (Fig. 4a). After heating in H_2 (Fig. 4b) and H_2S

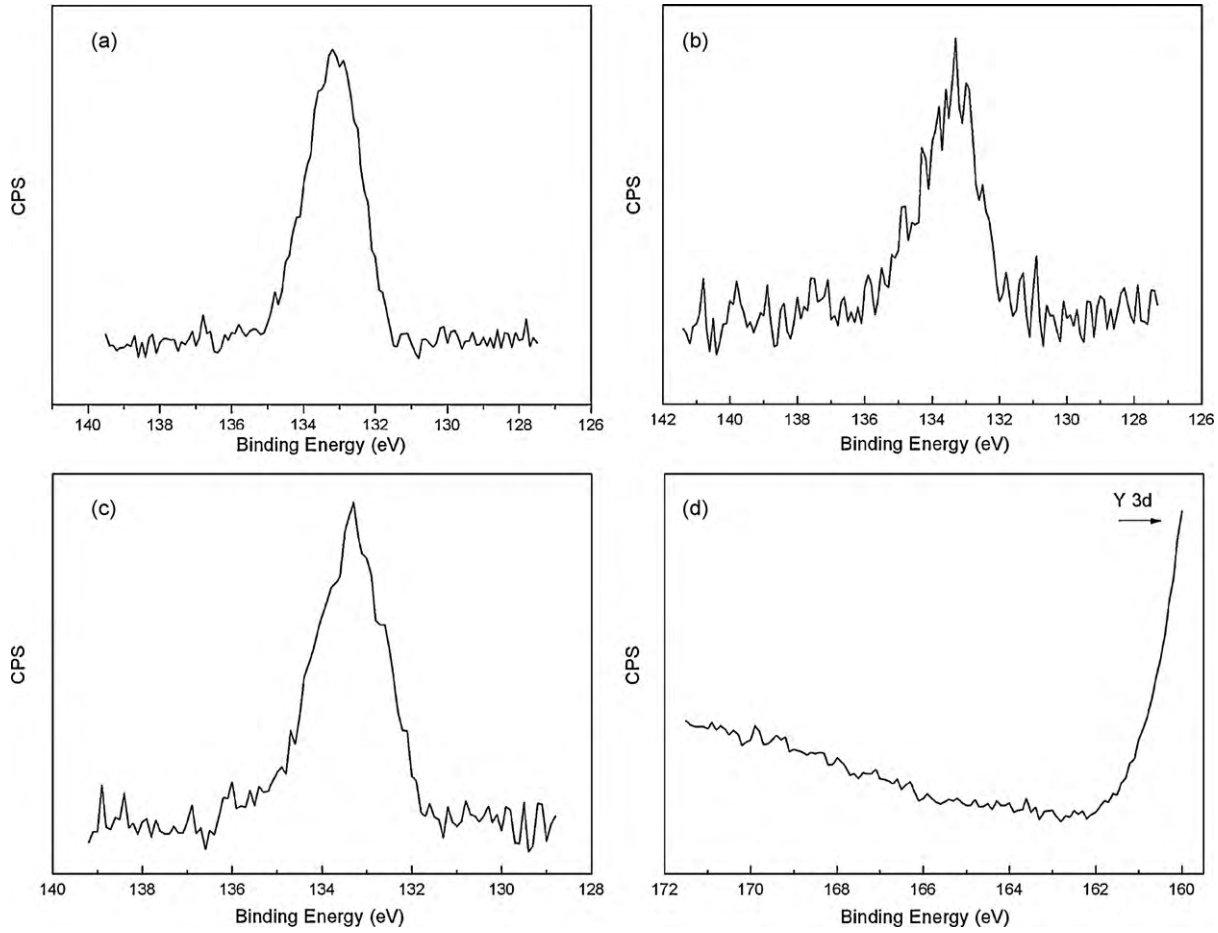

Fig. 4. XPS analysis of element P 2p and S 2p of YKC-12 composite: (a) fresh sample; (b) after test in H_2; (c) and (d) after tests in H_2S.

(Fig. 4c), the peak for P 2p was at the same location, which showed that the chemical environment of phosphorus was unchanged when the sample was heated in H_2 and H_2S atmospheres. Thus P had not been reduced by H_2 and phosphate had not reacted with H_2S to form P-S bonded species. In addition, Fig. 4d shows no peak for sulfur or any compound which contains sulfur in the range from 160 to 172 eV, demonstrating that there was neither a chemical reaction between constituents of the composite nor with H_2S. There was no detectable absorption of H_2S on the surface. Thus the XPS data showed the stability of YKC-12 composite in either H_2 or H_2S atmosphere at fuel cell operation temperatures.

Before testing with H_2S containing fuels, each cell was tested in H_2-air. In each case the OCV was above 1 V and stable. The potential was substantially the same as the theoretic value calculated from the Nernst equation, showing that there was no significant cross-over of hydrogen through the membrane.

3.2. Electrochemical properties

Impedance spectroscopy can resolve the bulk, grain-boundary and electrode processes in ceramic samples by exhibiting successive semicircles (often with some distortion) in the complex plane [12]. Normally, the high frequency arc corresponds to phenomena occurring in the bulk of the electrolyte (grain interior, R2 and CPE1 in Fig. 5), the mid-frequency arc is assigned to impedances associated with the microstructure of the ceramic electrolyte (i.e., the size and nature of grains and grain boundaries, R3 and C1 in Fig. 5) and the low-frequency arc represents the behavior occurring at the electrolyte-electrode interface (R4 and CPE2 in Fig. 5) [13]. However, all these contributions vary with temperature, and at some frequency ranges they may not all be found. Fig. 5 shows the impedance spectra for YKC-12 at different temperatures. The spectrum of the sample at 600 °C consisted of two semicircles, and these both shifted toward lower values when

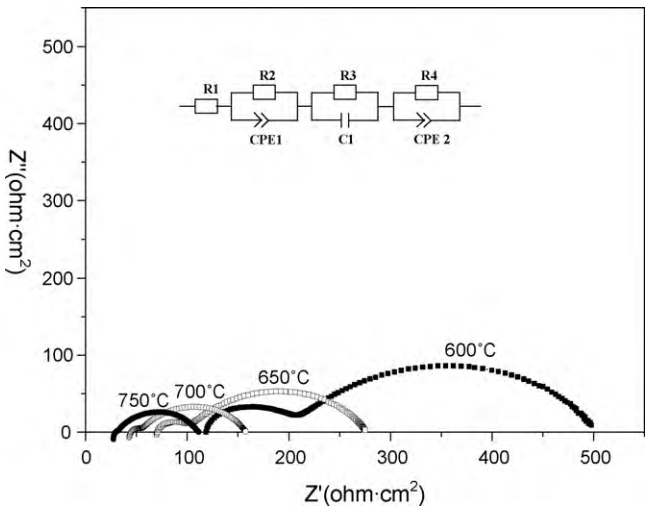

Fig. 5. Impedance spectra for YKC-12 in H_2 at various temperatures. Insert is the equivalent circuit used in modeling impedance.

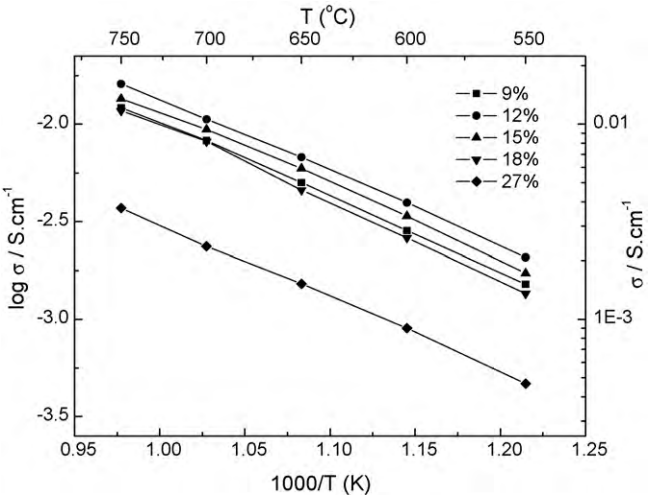

Fig. 6. Temperature dependence of conductivity of YSZ–K_3PO_4–$Ca_3(PO_4)_2$ composites with different phosphates weight ratios (9%, 12%, 15%, 18% and 27%) in H_2 atmosphere.

the temperature was increased. These two semicircles are ascribed to two thermally activated processes, ion transport within grain boundary and mass transfer at the electrolyte–electrode interface. With increase of temperature, the first semicircle steadily became smaller and less discernable until; finally, only one semicircle predominated in the spectra, ascribable to a relatively high grain boundary conductivity. At the same time, the second semicircle become smaller with the increase of temperature, ascribable to more rapid mass transfer at the electrolyte–electrode interface at high temperature.

The conductivities of YSZ–K_3PO_4–$Ca_3(PO_4)_2$ composites at various temperatures in H_2 were determined using the equivalent circuit illustrated in Fig. 5. Fig. 6 shows the total ionic conductivity of the composites with different binary phosphate weight ratios (9%, 12%, 15%, 18% and 27%) in the temperature range 550–750 °C under H_2. The activation energies over samples with different weight ratios were almost the same (8.06E3 kJ), suggesting the same conducting mechanism. YKC-12 had the highest conductivity among the compositions tested. Increasing or decreasing the proportion of phosphate led to a decrease in conductivity. The conductivity increased with temperature. At 700 °C the conductivity of the YKC-12 was 1×10^{-2} S cm^{-1}, a value which is promising for H_2S fuel cell applications.

The proton transport number of YKC-12 composite was measured at 550–750 °C in a hydrogen concentration cell using Pt paste as both electrodes (Fig. 7). The composite material showed high proton transport number above 90% over the whole temperature range, with a peak value about 99% at 700 °C.

It is widely known that YSZ has high oxygen ion conductivity at high temperatures (typically > 800 °C). The proton conductivity of ionic phosphates also is relatively high, up to 10^{-3} S cm^{-1} [14]. The present data show that the proton conductivity of the composite is even higher than that of ionic phosphates alone. Currently, the detailed mechanism of proton conduction in these composite materials is still not clear.

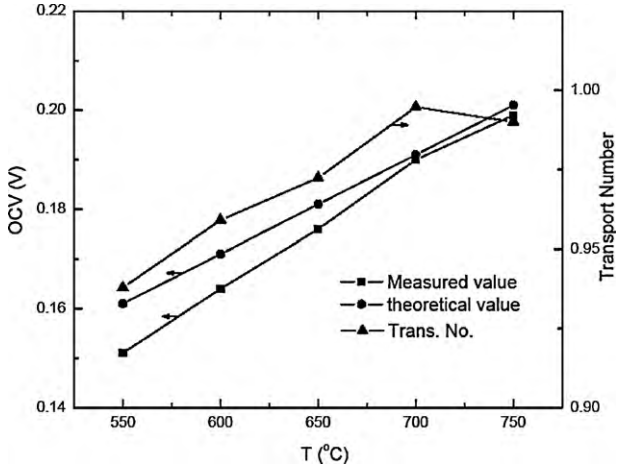

Fig. 7. Temperature dependence of proton transport numbers of YKC-12 composite.

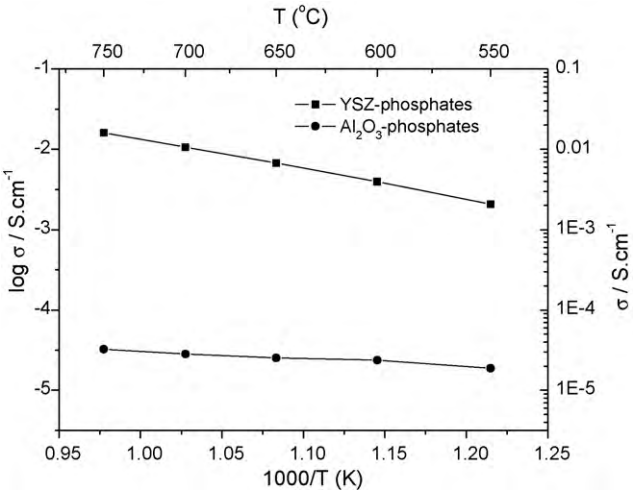

Fig. 8. Temperature dependence of conductivity of YKC-12 and AKC-12 composite.

However, there is some evidence for possible mechanisms [15,16]. Protons can be directly coordinated with phosphate to form hydrogen bonds. At the same time, in the interfacial area the protons can be readily bonded to the oxygen ion/atoms at the YSZ grain surfaces. Because of the high mobility of oxygen ions in YSZ, the captured protons can be released from one oxygen ion only to be captured again by a neighbor oxygen ion. In this manner, protons can be transported from one side to the other side by being sequentially captured and released by successive interfacial oxygen ions, thus enabling proton conductivity [15]. At the same time, oxygen ions are prevented from being conducted between the YSZ grains because they are covered with the phosphate material which acts as an oxide ion insulator.

To test this proton conducting mechanism, a known oxide having very low oxide ion conductivity, alumina, was intimately admixed with K_3PO_4–$Ca_3(PO_4)_2$. Fig. 8 compares the conductivity of YKC-12 composite and Al_2O_3–K_3PO_4–$Ca_3(PO_4)_2$ (12 wt%) composite (abbreviated as AKC-12 hereafter). The conductivity of composite was much lower than that of YKC-12 composite. The difference is attributed to alumina not having the same oxygen vacancies as YSZ, thus restricting the mobility of the oxygen ions. Consequently, AKC-12 composite has no capability to conduct protons by the interface within the composite, and so proton conductivity was low, having only that proton conductivity contributed by the phosphate component.

In this mechanism, the surfaces of YSZ grains play an important role in proton conduction, therefore higher conductivity can be achieved by reducing the sizes of YSZ grains. However, the grain size of the present electrolyte prepared by sintering pellets after a dry-pressing process is of the order of micrometers, and so the total surface area of the grains is limited. It is anticipated that use of the same materials with smaller grain size, and in particular nanograins, using appropriate preparation methods, will enhance performance of the electrolyte for application in SOFCs. Thus it is desirable to use the smallest available YSZ particles to maximize the surface area, hence our use of nanoparticles.

4. Conclusions

A new type of proton conductive ceramic-salt composite electrolyte, YSZ–K_3PO_4–$Ca_3(PO_4)_2$, has potential utility as an electrolyte in fuel cells using H_2S containing feeds. The composite electrolyte is stable in H_2S and H_2 atmospheres at temperatures 550–750 °C. Composites comprising 12 wt% binary phosphates-YSZ have high conductivity (1×10^{-2} S cm^{-1}) and high proton transport number (about 99%) at 700 °C. Use of nanoparticles of YSZ maximizes available surface area and thus also performance of the composite electrolyte.

Acknowledgment

This work was supported by Natural Sciences and Engineering Research Council of Canada (NSERC) Strategic Project Grant.

References

[1] N.U. Pujare, K.W. Semkow, A.F. Sammells, J. Electrochem. Soc. 134 (1987) 2639.
[2] I. Yentekakis, C. Vayenas, J. Electrochem. Soc. 136 (1989) 996.
[3] D. Peterson, J. Winnick, J. Electrochem. Soc. 145 (1998) 1449.
[4] R. Mukandan, E. Brosha, F. Garzon, Electrochem. Solid-State Lett. 7 (2004) A5.
[5] X. Xu, C. Xia, S. Huang, D. Peng, Ceram. Inter. 31 (2005) 1061.
[6] X. Liu, G. Li, J. Tong, D. Chen, Ceram. Inter. 30 (2004) 2057.
[7] T. Schober, H. Ringel, Ionics 10 (2004) 391.
[8] A. Lunde, B.-E. Mellander, B. Zhu, Acta Chem. Scand. 45 (1991) 981.
[9] B. Zhu, High-Perform. Ceram. III 280–283 (Pts 1 and 2) (2005) 413.
[10] G.L. Wei, J.L. Luo, A.R. Sanger, K.T. Chuang, L. Zhong, J. Power Sources 145 (2005) 1.
[11] B.H. Wang, J.D. Wang, R.Q. Liu, Y.H. Xie, Z.J. Li, J. Solid State Electrochem. 11 (1) (2006) 27.
[12] J.E. Bauerle, J. Phys. Chem. Solids 30 (1969) 2657.
[13] S.D. Flint, M. Hartmanova, J.J. Jones, R.C.T. Slade, Solid State Ionics 86–88 (1996) 697.
[14] B.-E. Mellander, B. Zhu, Solid State Ionics 61 (1993) 105.
[15] B. Zhu, M.D. Mat, Int. J. Electrochem. Sci. 1 (2006) 383.
[16] T. Schober, Electrochem. Solid-State Lett. 8 (4) (2005) A199.